Insulator-metal transition and crossover from negative to positive magnetoresistance in Cu$_2$IrO$_3$ under high pressure

Cheng Jin,[1] Yonggang Wang,[1,*] Meiling Jin,[2] Zimin Jiang,[1] Dequan Jiang,[1] Junlong Li,[1] Yuki Nakamoto,[3]
Katsuya Shimizu,[3] and Jinlong Zhu ®[1,2,†]

[1]*Center for High Pressure Science and Technology Advanced Research (HPSTAR), Beijing, 100094, China*

[2]*Department of Physics, Southern University of Science and Technology, Shenzhen, 518055, China*

[3]*Center for Science and Technology under Extreme Conditions, Graduate School of Engineering Science, Osaka University,
1–3 Machikaneyama-Cho, Toyonaka, Osaka, 560–8531, Japan*

Quantum spin liquid (QSL) state has attracted a great deal of attention as a precursor of high-temperature superconductor. The promising QSL candidates such as α-RuCl$_3$, Na$_2$IrO$_3$ and α-Li$_2$IrO$_3$ with honeycomb structure are insulators or semiconductors. An insulator-metal transition (IMT) is necessary for hosting superconducting state. However, all of them have a robust insulating state, even under pressure. Here, an alternative candidate of QSL, Cu$_2$IrO$_3$ is investigated under high pressure and low temperature through x-ray diffraction and electric properties measurement. A dimerization occurs at 7.1 GPa which is similar to α-RuCl$_3$ and α-Li$_2$IrO$_3$, accompanied with an anomaly of resistance at $\sim$5.0 GPa. The IMT appears under a pressure of $\sim$13.8 GPa, which is absent in α-RuCl$_3$, Na$_2$IrO$_3$ and α-Li$_2$IrO$_3$ under pressure. It is related to the crystal structure transition at $\sim$11.1 GPa, which induces the decline of interlayer distance. Furthermore, a strange crossover from negative to positive magnetoresistance is observed under pressure of 21.8 to 24.2 GPa at 2 K. This may be due to the valence change of Cu$^+$ to Cu^{2+}, as a result of the decreasing of interlayer distance and the shortening of O–Cu–O bond under pressure.

I. INTRODUCTION

In the past decade, $4d/5d$ transition-metal compounds with layered honeycomb structure, for instance α-RuCl$_3$ [1–3], Na$_2$IrO$_3$ [4–6], α-Li$_2$IrO$_3$ [7–9], and the Cu$_2$IrO$_3$ studied here, have attracted great interest as their promising systems hosting potential quantum spin liquid (QSL) state referring to the Kitaev model [10]. Theoretically, QSLs are predicted to be the precursor of new-typed high-temperature superconductor [11]. Generally speaking, $4d/5d$ transition-metal compounds have a weaker Coulomb interaction potential U and a larger bandwidth W comparing with $3d$ transition-metal compounds, and a metallic conductivity is expected. However, strange insulating states appear in α-RuCl$_3$, Na$_2$IrO$_3$, α-Li$_2$IrO$_3$, Cu$_2$IrO$_3$, etc. These phenomena come from the strong spin-orbit coupling (SOC), although they disobey the $U > W$ Mott criterion [12]. SOC drives the Ru ($4d$) or Ir ($5d$) t_{2g} orbitals splitting near the Fermi level and form bands with effective angular momenta $J_{\text{eff}} = 1/2$ and $J_{\text{eff}} = 3/2$; then, a small U can open a Mott gap E_g in the $J_{\text{eff}} = 1/2$ band, forming an upper Hubbard band (UHB) and lower Hubbard band (LHB) [6]. In order to get metallic conductive phase and further possible high-temperature superconductor, an insulator-metal transition (IMT) should occur modulated by

external interventions, such as temperature, magnetic/electric field, doping, pressure, etc. [13–15].

As a "clean" method, pressure can effectively tune the crystal structure of matters in means of changing lattice parameters, bond lengths, bond angles, and even space group, inducing electric structure or crystal structure transitions. Specifically, pressure can induce the band-structure transformation, band shifting, and band-gap closing. In previous research, Bastien *et al.*'s work showed a dimerization accompanying with a magnetic collapse under pressure near 0.2 GPa using magnetization and high-resolution x-ray diffraction measurements. Theoretical calculations indicated that dimerization enhanced the direct $4d$–$4d$ bonding on particular Ru-Ru links and caused a sharp increasing of the antiferromagnetic exchange interaction [2]. Transporting properties of Sun *et al.*'s work supported that α-RuCl$_3$ had a robust insulating state upon to 139.7 GPa, although theoretical calculation predicted a band-gap closure at $\sim$15 GPa [3]. Similarly, α-Li$_2$IrO$_3$ was confirmed to cause dimerization and magnetic collapse at the pressures of 3.8 and 4.1 GPa through high-pressure x-ray diffraction (XRD) and Raman spectroscopy [7,9]. In electric properties, Na$_2$IrO$_3$ and α-Li$_2$IrO$_3$ also show an insulator up to $\sim$80 and $\sim$55 GPa, respectively [6,16]. New kinds of Kitaev materials which host IMT under high pressure are still limited.

In this work, a Cu$_2$IrO$_3$, which has a 2D layered honeycomb structure with IrO$_6$ octahedral sharing the edge in the layer, just the same as Na$_2$IrO$_3$ and α-Li$_2$IrO$_3$, is selected for high-pressure study (Fig. 1). It has a monoclinic

*yonggang.wang@hpstar.ac.cn
†jinlong.zhu@hpstar.ac.cn
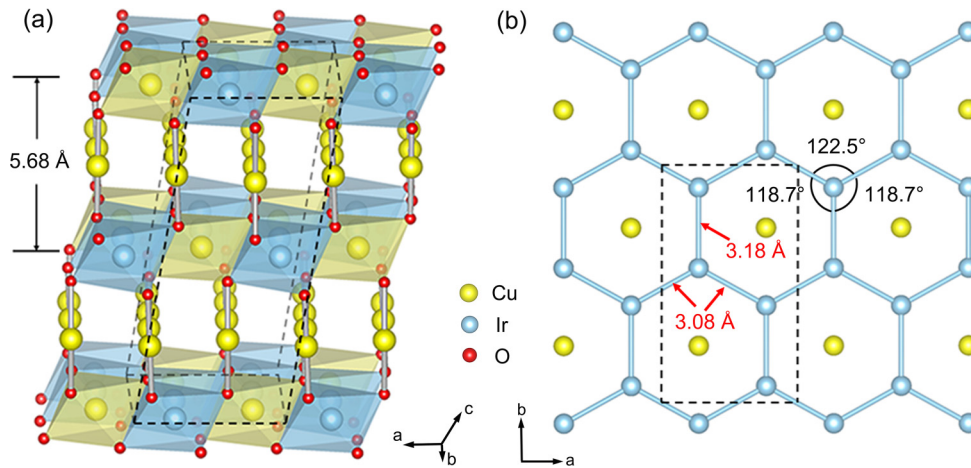
FIG. 1. The crystal structure of Cu_2IrO_3 at ambient conditions. (a) the layered honeycomb structure; (b) the *ab* plane of honeycomb layer. All the values marked in the figure come from Ref. [17].

space group ($C2/c$) with lattice parameters of $a = 5.39$ Å, $b = 9.31$ Å, $c = 11.51$ Å, and $\beta = 99.03°$ at ambient conditions. Its Ir–Ir–Ir bond angles in the intralayer are even closer to $120°$ than that in Na_2IrO_3, therefore in closer proximity to the geometry of the Kitaev model [Fig. 1(b)]. Differently, the presence of O–Cu–O dumbbell bonds in the interlayer connects the honeycomb layers and the interlayer distance is 5.68 Å [17] [Fig. 1(a)]. The resistance measurement showed a semiconducting behavior, and the magnetic susceptibility as a function of temperature indicated that there is no long-range magnetic ordering [17]. In the research of Ref. [18], the muon spin regulation (μSR) and x-ray absorption spectroscopy (XAS) suggested a coexistence of Cu^+/Cu^{2+} and Ir^{4+}/Ir^{3+}, which leads to the coexistence of Kitaev QSL state and static magnetism. The Cu^{2+}/Ir^{3+} ions are separated in the regions of static magnetism, whereas the Cu^+/Ir^{4+} ions form areas of Kitaev QSL in the honeycomb layer [18]. High-field NMR research demonstrated that its spin susceptibility behaves nearly identically to Na_2IrO_3, without showing evidence of magnetic ordering at low temperatures. It was also shown that the upturn of susceptibility below $T = 50$ K is from the contribution of defect spins [19]. The nuclear quadrupole resonance experiment at Ir^{4+} sites supported that spin fluctuations of Ir atoms exhibit no evidence for critical slowing down toward magnetic long-range order in zero external magnetic field. Moreover, the low-energy spin-excitation spectrum is dominated by a mode that has a large excitation gap comparable to the Ising interactions, a signature expected for Majorana fermions of the Kitaev quantum spin liquid [20]. Choi *et al.*'s work in $C_m(T)$ and μSR found no indication of spin glass down to 260 mK [21]. So, it is worthy to explore the proximate Kitaev QSL state of Cu_2IrO_3. More recently, Fabbris *et al.*'s work in high-pressure XRD and low temperature showed that dimerization occurred below 8 GPa at both ambient and low temperature in Cu_2IrO_3. Under pressure of 15 GPa and at room temperature, another phase transition appeared, which was induced by large discontinuous reduction of the Ir honeycomb interplanar distance and was likely driven by a collapse of the O–Cu–O dumbbell bonds [22]. However, research on electric properties upon compression is still lacking.

In our work, a dimerization at $\sim$7.1 GPa and a second crystal structure transition at $\sim$11.1 GPa were observed. For the transporting measurement, the first transition was observed at $\sim$5.0 GPa and IMT occurred at $\sim$13.8 GPa, which is consistent with the crystal structure transitions. At 2 K, a strange crossover from negative to positive magnetoresistance appeared under pressure of $\sim$21.8 to 24.2 GPa.

II. METHODS

A. Synthesis of Cu_2IrO_3 sample

Polycrystalline Cu_2IrO_3 was obtained through a metathesis reaction between sodium iridate (Na_2IrO_3) and copper (I) chloride (CuCl, Aladdin, 97%). The precursor Na_2IrO_3 was synthesized by solid-phase sintering of sodium carbonate (Na_2CO_3, Aladdin, 99.5%) and iridium oxide (IrO_2, Aladdin, 99.9% metal basis, Ir $\geqslant$ 84.5%). After a well ground in an agate mortar, the homogeneous mixture with the mole ratio of 1.15:1 was placed in a covered alumina crucible and heated in a muffle furnace under 800 °C for 24 h and then at 825 °C for 12 h. This presintering procedure was repeated twice, 24 h in total. The final sintering was carried out in a vacuum tube furnace for 24 h and the powder Na_2IrO_3 was transferred to a glove box immediately. Afterwards, Na_2IrO_3 and CuCl, with the mole ratio of 1:3, were ground in the glove box, placed in a covered alumina crucible, and sealed under vacuum in a quartz tube. The quartz tube was heated to 350 °C and held for 16 h. The product was washed three times with ammonium hydroxide (NH_4OH, Sinopharm, 28%) and twice with deionized water. After being washed, samples were dried at 70 °C in air-dry oven for 12 h [17].

B. X-ray diffraction at ambient conditions

Powder x-ray diffraction (XRD) measurement at ambient conditions was performed on a Bruker D8 advance diffractometer at 60 kV, 300 mA by using Cu K_α radiation ($\lambda = 1.5406$ Å), with a scan speed of 5° min^{-1} and a step size of 0.02° in 2θ. The x-ray powder diffraction (XRPD) pattern and Rietveld refinement by employing the initial structure from
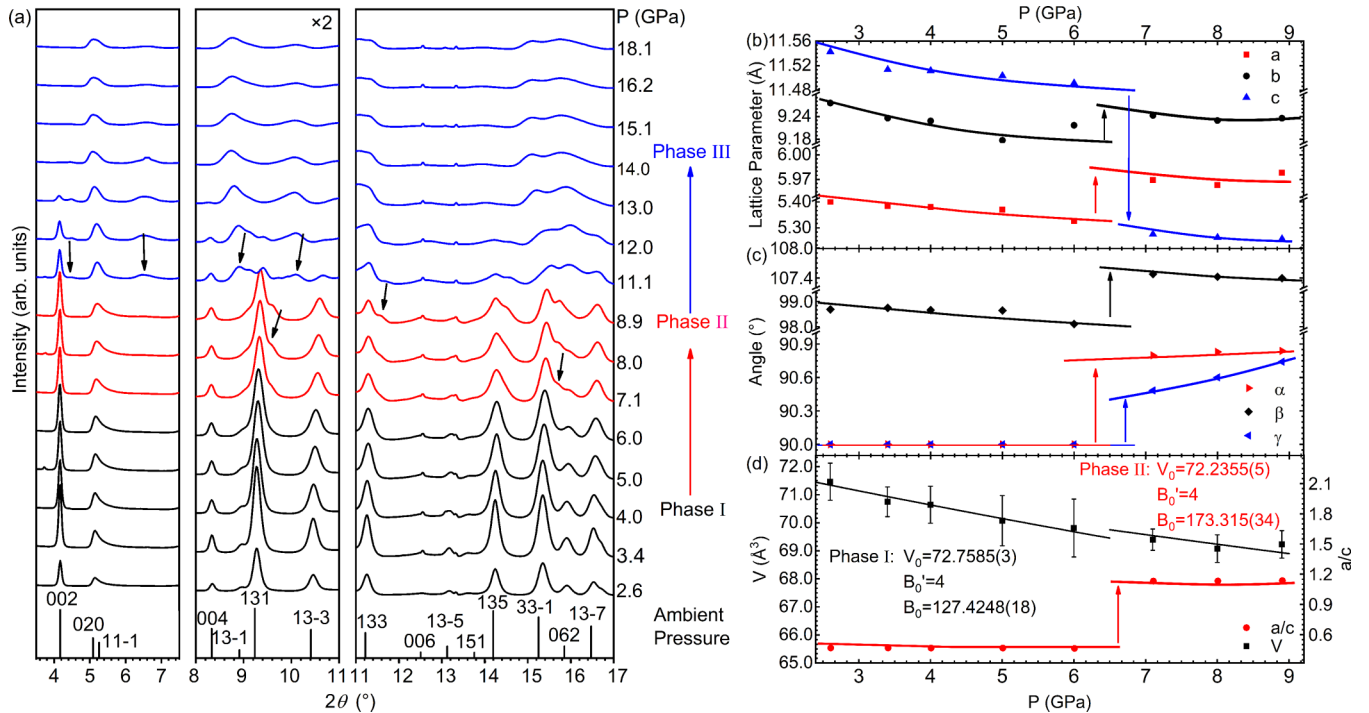
FIG. 2. (a) The XRD data of Cu_2IrO_3 under the pressure of 2.6 to 18.1 GPa. The bottom plots the calculated standard spectrum of Cu_2IrO_3 at ambient conditions. The black arrows mark the new peaks emerging during the phase transitions. (b)–(d) show the evolution of lattice parameters and unit-cell volume as a function of pressure. The lines and arrows are plotted for the guiding of sight except for the unit-cell volume in (d). The unit-cell volume is fitted by the second-order BM EOS and the black line is the fitting result. B_0' is fixed to be 4. $B_0 = 127.4248(18)$ GPa, $V_0 = 72.7585(3)$ Å^3 in phase I and $B_0 = 173.315(34)$ GPa, $V_0 = 72.2355(5)$ Å^3 in phase II.

Ref. [17] are plotted in Fig. S1 [23]. The result indicated a high quality of the as-synthesized sample.

C. High-pressure synchrotron XRD

High-pressure synchrotron XRD experiments were carried out at SPring-8 BL10XU ($\lambda = 0.4129$ Å) in Japan by a symmetric-typed diamond-anvil cell (DAC) with a diamond culet of 300 μm. A T301 stainless-steel gasket was compressed to the thickness of $\sim$38 μm and drilled a center hole with a diameter of 150 μm to be the sample chamber. Pressure was calibrated by fluorescence of ruby balls with a size of $\sim$10-μm diameter [24] and a mineral oil was used as pressure-transmitting medium. The two-dimensional diffraction patterns were collected by an x-ray flat-panel detector and integrated to 2θ versus intensity data using the DIOPTAS software [25]. Rietveld refinement of the XRD patterns were performed by applying GSAS+EXPGUI software packages [26].

D. Transporting measurements at high pressure and low temperature

The high-pressure and low-temperature electronic transport properties of Cu_2IrO_3 samples were measured through the Van der Pauw method in DACs made of CuBe alloy. The diamond culet was 300 μm and the Au wires with a diameter of 18 μm were used as electrodes. A T301 stainless-steel nonmagnetic gasket was pressed to $\sim$32-μm thickness and then drilled a center hole with a diameter of 180 μm. The cubic boron nitride (c-BN) was pressed in the hole up to

the pressure of 20 GPa as an insulating layer. A small center hole with diameter of 80 μm was further drilled as the sample chamber and NaCl fine powder was loaded serving as pressure-transmitting medium. A piece of Cu_2IrO_3 with dimensions of 50 μm × 50 μm × 10 μm (pressed polycrystal sample) was loaded and ruby balls were just loaded near the sample as pressure markers [24]. The DAC was placed in the C-mag system with automatic temperature control.

III. RESULTS AND DISCUSSION

A. Dimerization and crystal structure transitions under pressure

The synchrotron XRD patterns up to 18.1 GPa were plotted in Fig. 2. The region of 2θ from 5° to 6° in Fig. 2 or from 19° to 22° in Fig. S1(a) showing an asymmetric peak, known as the Warren line shape, is original from the stacking faults between layers [17], which is similar as in $H_3LiIr_2O_6$ [27] and $Ag_3LiIr_2O_6$ [28]. Upon compression to 18.1 GPa, two phase transitions at $\sim$7.1 to 8.9 GPa and $\sim$11.1 GPa are observed. For the phase transition from phase I to phase II, three shoulders at 15.7°, 9.6°, and 11.6° appear at pressures of 7.1, 8.0, and 8.9 GPa, respectively. As a result, the crystal structure can no longer be refined with monoclinic space group $C2/c$. It requires a triclinic space group $P\bar{1}$ in phase II [22]. The pressure dependence of the lattice parameters and unit-cell volume is shown in Figs. 2(b)–2(d). The details of Rietveld refinement at 0 GPa ($C2/c$) and 8.0 GPa ($P\bar{1}$) are shown in Fig. S1 and Tables S1 and S2 [23]. The huge decrease of c axis between phase I and phase II is due to the choice of unit cell,
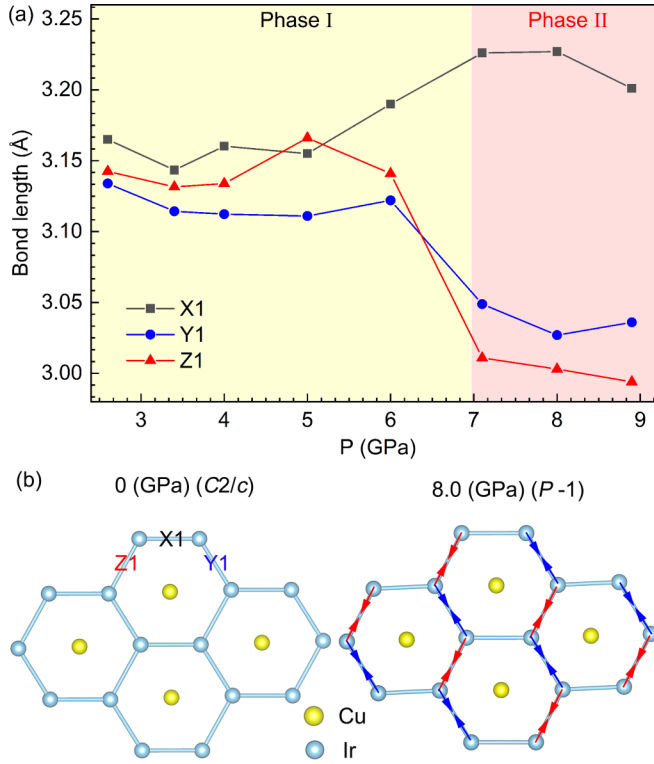
FIG. 3. (a) The evolution of Ir-Ir bond lengths under pressure from 2.6 to 8.9 GPa. X1, Y1, and Z1 correspond to the Ir—Ir bond at different positions shown in (b). (b) The in-plane honeycomb structure at 0 GPa ($C2/c$) and 8.0 GPa ($P\bar{1}$). The red and blue arrows mark the dimerization at Z1 position and Y1 position, respectively.

in which $Z = 8$ and $Z = 4$, respectively. In Fig. 2(d), the unit-cell volume is fitted with the second-order Birch-Murnaghan (BM) equation of state (EOS) [22]:

$$P = \frac{3B_0}{2}\left[\left(\frac{V}{V_0}\right)^{-(7/3)} - \left(\frac{V}{V_0}\right)^{-(5/3)}\right]$$
$$\times \left\{1 + \frac{3}{4}(B_0' - 4)\left[\left(\frac{V}{V_0}\right)^{-(2/3)} - 1\right]\right\}, \quad (1)$$

where V_0 is the ambient volume per formula unit, V is the volume per formula unit at pressure P given in GPa, B_0 is the bulk modulus, and B_0' is the derivative of bulk modulus. B_0' is fixed to be 4 as the few experimental data points for each phase. In the fitting results, it gives the bulk modulus $B_0 = 127.4248(18)$ GPa, $V_0 = 72.7585(3)$ Å^3 of phase I and $B_0 = 173.315(34)$ GPa, $V_0 = 72.2355(5)$ Å^3 of phase II. This indicates an obvious hardening from phase I to phase II.

In order to provide more information of the phase transitions, the refined Ir–Ir bond lengths evolution depending on pressure are shown in Fig. 3(a). At ambient pressure, Cu$_2$IrO$_3$ has a nearly perfect hexagonal lattice, which has three typed Ir–Ir bonds, marked as X1, Y1, Z1 in Fig. 3(b). On the contrary, phase II indicates an obvious dimerization, which also can be observed in similar honeycomb structure, as in α-RuCl$_3$ [2], Li$_2$RuO$_3$ [29], and α-Li$_2$IrO$_3$ [7]. Generally, there are two types of dimerization in honeycomb structure armchair(herringbone)-type arrangement and ladder parallel-type arrangement. In Cu$_2$IrO$_3$, dimerization happens

on the Y1 bond and Z1 bond [Fig. 3(b)] according to the refinement result. At 7.1 GPa, the bond lengths of X1, Y1, and Z1 are 3.23, 3.03, and 3.01 Å, respectively. Similarly, in Li$_2$RuO$_3$ with a $P2_1/m$ space group preserving of C_2 axis, its dimerization also exists on both Y1 position and Z1 position. The length of X1-typed long Ir–Ir bonds is ∼3.1 Å and the length of Y1/Z1-typed short Ir–Ir bonds is 2.55 Å, leading to a difference of ∼0.55 Å. Conclusively, both Cu$_2$IrO$_3$ and Li$_2$RuO$_3$ have an armchair(herringbone)-type arrangement of dimers, which is different from the x-ray absorption fine-structure data in Ref. [22]; this needs more evidence to go further. Differently, in α-RuCl$_3$, its dimerization occurs on Z1-typed Ir–Ir bonds and induces a great difference between long Ru-Ru (X1 and Y1, 3.53 Å) and short Ru-Ru (Z1, 2.86 Å) of ∼0.7 Å. In α-Li$_2$IrO$_3$, dimerization occurs on either Y1-typed or Z1-typed Ir–Ir bonds and has a difference of 3.00 (Z1)−2.69 (X1 or Y1) = 0.31 Å. The latter two situations belong to another arrangement of dimers: ladder parallel. The different arrangements result in energy difference. According to the discussion in Refs. [29,30], the choice of arrangement depends on long-range interaction, such as elastic interaction.

Phase III emerged at 11.1 GPa with several significant changes of Bragg peaks. Peaks at 4.5°, 6.5°, 8.9°, and 10.1° are observed simultaneously. Although we did not refine the crystal structure successfully, the discontinuous increase of the Bragg peak at $2\theta \sim 4°$ means a collapse of interplanar distance [Fig. 2(a)]. The theoretical calculation in Ref. [22] had a similar conclusion, showing a decreasing of interlayer distance at 15.1 GPa [22]. This may result from the buckling of O–Cu–O dumbbells or shortening of Cu–O bonds under pressure. Further, dimerization and collapse of interlayer distance are closely related to the electric properties transferring.

B. Insulator-metal transition and resistance minimal value under pressure

Dimerization and collapse of interplanar distance accompany the changes of bond lengths and bond angles of Ir–Ir–Ir and O–Cu–O, having significant impact on the physical properties. For instance, dimerization in α-RuCl$_3$ [2] and α-Li$_2$IrO$_3$ [7] is accompanied by magnetic collapse [2,9]. To investigate evolution of electric properties, we continue to carry out the transporting measurements under high pressure and at low temperature. Figure 4(a) plots the pressure dependence of resistance from 0 to 26.8 GPa at room temperature. Resistance decreases under compression initially and the first anomaly of resistance occurs at ∼5.0 GPa, turning to increase with further increasing of pressure. Then, a huge drop appears in the small region from 10.0 to 13.8 GPa. At last, a minimal value of resistance is observed at pressure of 21.8 to 24.2 GPa just as the insets of Figs. 4(a), 4(b), and 4(c) show the temperature dependence of resistance under pressure of 0 to 26.8 GPa at temperature down to 2 K. Below 13.8 GPa, resistance increases upon cooling, indicating an insulating behavior. Compressing upon 13.8 GPa, an IMT occurs and resistance transforms to decrease with reducing of temperature. It is unlike transporting in α-RuCl$_3$ [3], Na$_2$IrO$_3$ [6,16], and α-Li$_2$IrO$_3$ [16], which preserve a robust insulating state under pressure up to 139.7, 80, and 55 GPa, respectively. Besides, an upturn of resistance at ∼15 K exists in metallic phase, which
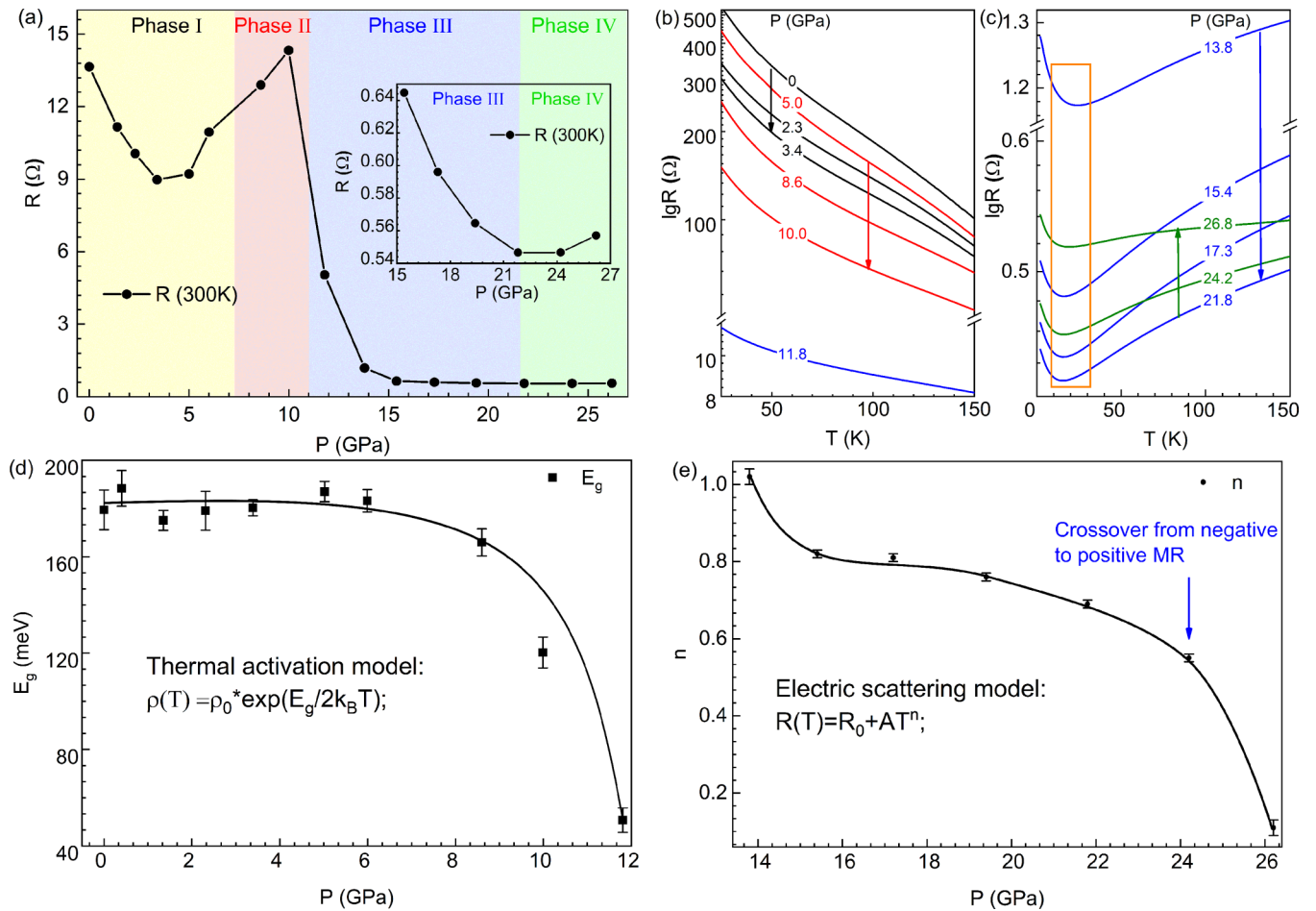
FIG. 4. (a) The evolution of resistance at the pressure of 0–26.8 GPa at 300 K. The inset plots the enlarged resistance evolution from 15 to 27 GPa. (b), (c) The temperature-dependent resistance under different pressures. The different colors mark different phases corresponding to (a) and the arrows are plotted for the guidance of sight. The anomalies below 25 K marked by orange square are related to Kondo effect. (d) The fitting result of thermal activation model below 11.8 GPa before the IMT at 250–300 K. E_g is the band gap. The line is just for the guidance of sight. (e) The fitting result of electric scattering model at metallic phase at 30–100 K. $n = 1$ means the non-Fermi liquid state. The line is just for the guidance of sight.

is robust against compression. Through carefully checking the resistance below 15 K, it can be found that the resistance obeys a logarithmic temperature dependence just as shown in Fig. S2 [23]. Therefore, this situation can be recognized as the impact of Kondo effect [31]. Kondo effect is original from scattering of magnetic impurities. The NMR study shows that there existed defect spins below 50 K [18]. The μSR and XAS experiment indicated the coexistence of static magnetism and Kitaev QSL [19]. All of these supported the appearance of magnetic impurities.

The resistance minimal value at 5.0 GPa is almost coincident with dimerization, indicating that resistance anomaly is closely related to dimerization. It is easy to understand that dimerization induces adjusting of Ir–Ir (Ru–Ru) bond lengths and Ir–Ir–Ir (Ru–Ru–Ru) bond angles in the honeycomb structure. These changes result in the reconstruction of d orbitals and breaking down of original electric ground state. In 4d compounds α-RuCl$_3$, compression enhances the covalent interaction and valence bond orbital forms accompanied by the dimerization [2]. In the 5d compounds α-Li$_2$IrO$_3$, dimerization occurs together with a breakdown of quasimolecular

orbital (QMO) and the energy-level scheme appears similar to the dimerized molecular orbital state of Li$_2$RuO$_3$ [8]. These indicate that dimerization can lead to the localization of electrons and increasing of resistance once phase transition has happened.

Accordingly, IMT at 13.8 GPa is closely related to the second crystal structure transition. On the basis of energy bond theory, IMT is related to the transitions of energy bands and band gap. Figure 4(d) plots the band-gap evolution versus pressure before the IMT. Resistance at high-temperature region (above 250 K) can be well fitted by the thermal activation model: $\rho(T) = \rho_0 \times e^{E_g/2k_BT}$, where k_B is the Boltzmann constant and E_g is the band gap. An example fitting at 0 GPa is shown in Fig S3 [23]. At ambient pressure, the band gap $E_g \approx 179$ meV. With an increase of pressure, a drastic decline of E_g starts at ~8.6 GPa and the band gap rapidly goes to closure upon 11.8 GPa. In the simplest scenario of Wilson's theory, Wilson distinguished metal, semiconductor, and insulator based on the filling of the conduction band and the width of the forbidden band (band gap). External condition changes, particular to high pressure here, can lead to the closure of

band gap. [32,33] Based on the pillar work of Wilson, Mott considered the electron-electron correlation and successfully explained the insulating state in some $3d$ compounds [34]. The Coulomb interaction can open up a band gap and form UHB and LHB. The criterion of Mott insulator is the magnitudes of Coulomb interaction U and bandwidth W. Further, $4d/5d$ compounds have a strong spin-orbital coupling, which can split d orbital into $J_{eff} = 1/2$ and $J_{eff} = 3/2$. Meanwhile, U opens a band gap in the $J_{eff} = 1/2$ band, forming UHB and LHB [12]. In the IMT of Cu_2IrO_3, pressure induces the decreasing of interlayer distance, resulting in buckling of O–Cu–O dumbbells and shortening of Cu–O bonds. This will enhance the orbital hybridization of Cu $3d$ orbital and O $2p$ orbital, inducing the broadening of bands. Thereby, the overlap between conduction band and valence band occurs and eventually the closure of band gap.

At the pressure of 21.8 GPa, a minimum value of resistance at 300 K is observed. The power-law fitting $R(T) = R_0 + AT^n$ is done at 30–100 K in metallic phase as shown in Fig. 4(e). The magnitude of n stands for the scattering mechanism. The index n experiences a sharp decline near the minimum value of resistance. These may indicate a possible transition from phase III to phase IV. Generally, $n = 2$ indicates the materials is a Fermi liquid and $n < 2$ stands for a non-Fermi liquid. Previous research of non-Fermi liquid showed that the origin may lie in subtle effects of disorder in the sample and the diffusive motion of electrons resulting from the interaction among the itinerant electrons [35]. Therefore, sharp decline of index n may be related to the transition from Cu^+ to Cu^{2+}, which may also be the origin of the crossover from negative to positive magnetoresistance in the following discussion. Unfortunately, our high-pressure XRD patterns did not cover the pressure region of a possible third transition shown by electric property. More work on higher-pressure structure of Cu_2IrO_3 needs to be carried out to confirm the third phase transition.

C. Crossover from negative to positive magnetoresistance

To get more information of a possible third transition, the magnetoresistance (MR) is investigated under magnetic field at high pressure and low temperature. Surprisingly, an exotic crossover from negative to positive magnetoresistance appears. Just as plotted in Fig. 5, magnetoresistance at 2 K show a negative behavior with increasing of magnetic field at pressure of 13.8 GPa. At pressure of 21.8 GPa, it starts to transform from negative to positive behavior; a minimal value of magnetoresistance appears at near 50 kOe. Finally, a completely positive magnetoresistance is realized above pressure of 24.2 GPa. Theoretically, the negative MR is due to the delocalization of electrons by magnetic field. The increase in conductivity by magnetic field is proportional to $H^2 \tau_e^{3/2}$, where τ_e is the energy relaxation time of electrons when the magnetic field is small [36]. In the previous research of doped ferromagnetic ZnO, negative MR is attributed to the minimization of magnetic scattering and positive MR originates from p-p exchange-interaction induced Zeeman splitting in the conduction band and the suppression of electron hopping [37]. In Dirac semimetal Cd_3As_2, negative MR is due to chiral anomaly, which is closely related to the low charge density [38]. Just as we stated above, Cu_2IrO_3 contains two kinds
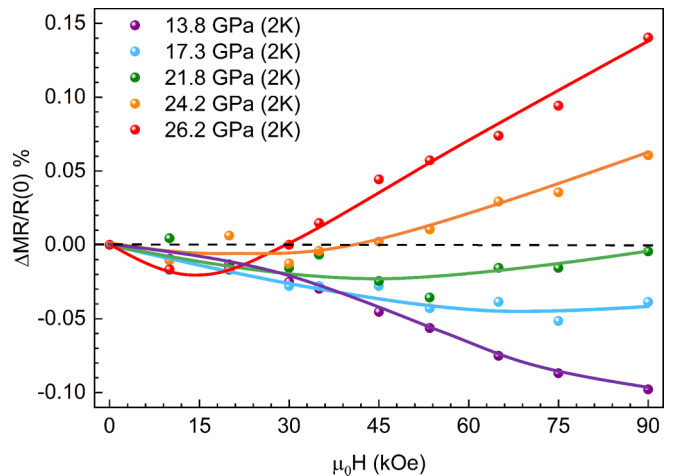
FIG. 5. The changing of magnetic field-dependent MR under different pressure in metallic phase at 2 K. The lines are just for the guidance of sight.

of Cu ions with the valence of +1 and +2, inducing static magnetism and Kitaev spin liquid, respectively. Cu^+ locates in the honeycomb layer and interlayer, while Cu^{2+} lies in the honeycomb layer only [18]. The magnetic ions Cu^{2+} ions are localized and minimize the magnetic scattering. As a result, Cu_2IrO_3 shows a negative MR. Pressure shortens the distance of interlayer and strengthens the Cu–O bonds; gradually Cu^+ ions transfer to Cu^{2+} ions. This means the delocalization of magnetic ions and strengthening of magnetic scattering. Consequently, a crossover from negative to positive MR occurs. The recent literature by Fabbris *et al.* [22] also indicated a crystal structure phase transition near 20 GPa under 10 K, which is caused by a collapse of interlayer distance. In the meantime, the theoretical calculation in Fabbris *et al.*'s work also supported the transition from Cu^+ to Cu^{2+} above 15 GPa [22].

IV. CONCLUSIONS

We have performed high-pressure XRD experiments and high-pressure and low-temperature transporting property measurements on polycrystalline Cu_2IrO_3. Firstly, a dimerization occurred at ~7.1 GPa, which may lead to the formation of molecular bond state. It is accompanied by a resistance minimal value in electric property. Then, the second crystal structure transition induced by decreasing of interlayer distance at ~11.1 GPa caused the closure of band gap. This results in an IMT upon 13.8 GPa in electronic property, which is not observed in the similar compounds of α-$RuCl_3$, Na_2IrO_3, and α-Li_2IrO_3. Lastly, a minimal value of resistance guided us to find a strange crossover from negative to positive magnetoresistance at 2 K under 21.8 GPa. It can be attributed to the transition from Cu^+ to Cu^{2+}, both of which coexist at the ambient pressure in Cu_2IrO_3.

[1] Y. Cui, J. Zheng, K. Ran, J. Wen, Z.-X. Liu, B. Liu, W. Guo, and W. Yu, High-pressure magnetization and NMR studies of α-RuCl$_3$, Phys. Rev. B **96**, 205147 (2017).

[2] G. Bastien, G. Garbarino, R. Yadav, F. J. Martinez-Casado, R. Beltrán Rodríguez, Q. Stahl, M. Kusch, S. P. Limandri, R. Ray, P. Lampen-Kelley *et al.*, Pressure-induced dimerization and valence bond crystal formation in the Kitaev-Heisenberg magnet α-RuCl$_3$, Phys. Rev. B **97**, 241108(R) (2018).

[3] Z. Wang, J. Guo, F. F. Tafti, A. Hegg, S. Sen, V. A. Sidorov, L. Wang, S. Cai, W. Yi, Y. Zhou *et al.*, Pressure-induced melting of magnetic order and emergence of a new quantum state in α-RuCl$_3$, Phys. Rev. B **97**, 245149 (2018).

[4] K. Hu, Z. Zhou, Y.-W. Wei, C.-K. Li, and J. Feng, Bond ordering and phase transitions in Na$_2$IrO$_3$ under high pressure, Phys. Rev. B **98**, 100103(R) (2018).

[5] V. Hermann, J. Ebad-Allah, F. Freund, I. M. Pietsch, A. Jesche, A. A. Tsirlin, J. Deisenhofer, M. Hanfland, P. Gegenwart, and C. A. Kuntscher, High-pressure versus isoelectronic doping effect on the honeycomb iridate Na$_2$IrO$_3$, Phys. Rev. B **96**, 195137 (2017).

[6] X. Xi, X. Bo, X. S. Xu, P. P. Kong, Z. Liu, X. G. Hong, C. Q. Jin, G. Cao, X. Wan, and G. L. Carr, Honeycomb lattice Na$_2$IrO$_3$ at high pressures: A robust spin-orbit Mott insulator, Phys. Rev. B **98**, 125117 (2018).

[7] V. Hermann, M. Altmeyer, J. Ebad-Allah, F. Freund, A. Jesche, A. A. Tsirlin, M. Hanfland, P. Gegenwart, I. I. Mazin, D. I. Khomskii, R. Valentí, and C. A. Kuntscher, Competition between spin-orbit coupling, magnetism, and dimerization in the honeycomb iridates: α-Li$_2$IrO$_3$ under pressure, Phys. Rev. B **97**, 020104(R) (2018).

[8] J. P. Clancy, H. Gretarsson, J. A. Sears, Y. Singh, S. Desgreniers, K. Mehlawat, S. Layek, G. K. Rozenberg, Y. Ding, M. H. Upton *et al.*, Pressure-driven collapse of the relativistic electronic ground state in a honeycomb iridate, npj Quantum Mater. **3**, 35 (2018).

[9] G. Li, L. L. Huang, X. Chen, C. Liu, S. Pei, X. Wang, S. Wang, Y. Zhao, D. Yu, L. Wang, F. Ye, J. Mei, and M. Huang, Probing the continuum scattering and magnetic collapse in single-crystalline α-Li$_2$IrO$_3$ by Raman spectroscopy, Phys. Rev. B **101**, 174436 (2020).

[10] A. Kitaev, Anyons in an exactly solved model and beyond, Ann. Phys. (N.Y.) **321**, 2 (2006).

[11] P. W. Anderson, The resonating valence bond state in La$_2$CuO$_4$ and superconductivity, Science **235**, 1196 (1987).

[12] G. Cao and L. De-Long (eds.), *Frontiers of 4d- and 5d-Transition Metal Oxides* (World Scientific, Singapore, 2013), pp. 1–5.

[13] D. Mandrus, J. R. Thompson, R. Gaal, L. Forro, J. C. Bryan, B. C. Chakoumakos, L. M. Woods, B. C. Sales, R. S. Fishman, and V. Keppens, Continuous metal-insulator transition in the pyrochlore Cd$_2$Os$_2$O$_7$, Phys. Rev. B **63**, 195104 (2001).

[14] A. Ohmura, A. Machida, T. Watanuki, K. Aoki, S. Nakano, and K. Takemura, Infrared spectroscopic study of the band-gap closure in YH$_3$ at high pressure, Phys. Rev. B **73**, 104105 (2006).

[15] H. Takami, T. Kanki, S. Ueda, K. Kobayashi, and H. Tanaka, Filling-controlled Mott transition in W-doped VO$_2$, Phys. Rev. B **85**, 205111 (2012).

[16] S. Layek, K. Mehlawat, D. Levy, E. Greenberg, M. P. Pasternak, J. P. Itié, Y. Singh, and G. Kh. Rozenberg, Electronic and structural properties of the honeycomb iridates A$_2$IrO$_3$ (A = Na, Li) at elevated pressures, Phys. Rev. B **102**, 085156 (2020).

[17] M. Abramchuk, C. Ozsoy-Keskinbora, J. W. Krizan, K. R. Metz, D. C. Bell, and F. Tafti, Cu$_2$IrO$_3$: A new magnetically frustrated honeycomb iridate, J. Am. Chem. Soc. **139**, 15371 (2017).

[18] E. M. Kenney, C. U. Segre, W. Lafargue-Dit-Hauret, O. I. Lebedev, M. Abramchuk, A. Berlie, S. P. Cottrell, G. Simutis, F. Bahrami, N. E. Mordvinova *et al.*, Coexistence of static and dynamic magnetism in the Kitaev spin liquid material Cu$_2$IrO$_3$, Phys. Rev. B **100**, 094418 (2019).

[19] J. Wang, High field NMR investigation of Kitaev spin liquid candidate Cu$_2$IrO$_3$, Ph.D. thesis, McMaster University, 2019, https://macsphere.mcmaster.ca/handle/11375/25060.

[20] S. K. Takahashi, J. Wang, A. Arsenault, T. Imai, M. Abramchuk, F. Tafti, and P. M. Singer, Spin Excitations of a Proximate Kitaev Quantum Spin Liquid Realized in Cu$_2$IrO$_3$, Phys. Rev. X **9**, 031047 (2019).

[21] Y. S. Choi, C. H. Lee, S. Lee, S. Yoon, W. J. Lee, J. Park, A. Ali, Y. Singh, J. Orain, G. Kim, J. Rhyee, W. Chen, F. Chou, and K. Choi, Exotic Low-Energy Excitations Emergent in the Random Kitaev Magnet Cu$_2$IrO$_3$, Phys. Rev. Lett. **122**, 167202 (2019).

[22] G. Fabbris, A. Thorn, W. Bi, M. Abramchuk, F. Bahrami, J. H. Kim, T. Shinmei, T. Irifune, F. Tafti, A. N. Kolmogorov, and D. Haskel, Complex pressure-temperature structural phase diagram of the honeycomb iridate Cu$_2$IrO$_3$, Phys. Rev. B **104**, 014102 (2021).

[23] See Supplemental Material at http://link.aps.org/supplemental/10.1103/PhysRevB.105.144402 for the detailed refinement results of different phase under pressure, the fitting of resistance at 21.8 GPa using logarithmic function, and the fitting of resistance at 0 GPa using thermal activation model at 250–300 K as an example.

[24] H. K. Mao, J. Xu, and P. M. Bell, Calibration of the ruby pressure gauge to 800 kbar under quasi-hydrostatic conditions, J. Geophys. Res.: Solid Earth **91**, 4673 (1986).

[25] C. Prescher and V. B. Prakapenka, DIOPTAS: A program for reduction of two-dimensional X-ray diffraction data and data exploration, High Pressure Res. **35**, 223 (2015).

[26] B. H. Toby, EXPGUI, a graphical user interface for GSAS, J. Appl. Crystallogr. **34**, 210 (2001).

[27] S. Bette, T. Takayama, K. Kitagawa, R. Takano, H. Takagi, and R. E. Dinnebier, Solution of the heavily stacking faulted crystal

structure of the honeycomb iridate $H_3LiIr_2O_6$, Dalton Trans. **46**, 15216 (2017).

[28] S. Bette, T. Takayama, V. Duppel, A. Poulain, H. Takagi, and R. E. Dinnebier, Crystal structure and stacking faults in the layered honeycomb, delafossite-type materials $Ag_3LiIr_2O_6$ and $Ag_3LiRu_2O_6$, Dalton Trans. **48**, 9250 (2019).

[29] S. A. J. Kimber, I. I. Mazin, J. Shen, H. O. Jeschke, S. V. Streltsov, D. N. Argyriou, R. Valentí, and D. I. Khomskii, Valence bond liquid phase in the honeycomblattice material Li_2RuO_3, Phys. Rev. B **89**, 081408(R) (2014).

[30] G. Jackeli and D. I. Khomskii, Classical Dimers and Dimerized Superstructure in an Orbitally Degenerate Honeycomb Antiferromagnet, Phys. Rev. Lett. **100**, 147203 (2008).

[31] J. Kondo, Resistance minimum in dilute magnetic alloys, Prog. Theor. Phys. **32**, 37 (1964).

[32] A. H. Wilson, The theory of electronic semi-conductors, Proc. R. Soc. London, Ser. A **133**, 458 (1931).

[33] A. H. Wilson, The theory of electronic semi-conductors-II, Proc. R. Soc. London, Ser. A **134**, 277 (1931).

[34] N. F. Mott, The basis of the electron theory of metals, with special reference to the transition metals, Proc. Phys. Soc. London, Sect. A **62**, 416 (1949).

[35] C. Pfleiderer, S. R. Julian, and G. G. Lonzarich, Non-Fermi-liquid nature of the normal state of itinerant-electron ferromagnets, Nature (London) **414**, 427 (2001).

[36] A. Kawabata, Theory of negative magnetoresistance in three-dimensional systems, Solid State Commun. **34**, 431 (1980).

[37] Y. Wang, X. Luo, L. T. Tseng, Z. Ao, T. Li, G. Xing, N. Bao, K. Suzukiis, J. Ding, S. Li, and J. Yi, Ferromagnetism and crossover of positive magnetoresistance to negative magnetoresistance in Na-doped ZnO, Chem. Mater. **27**, 1285 (2015).

[38] H. Li, H. He, H. Z. Lu, H. Zhang, H. Liu, R. Ma, Z. Fan, S. Shen, and J. Wang, Negative magnetoresistance in Dirac semimetal Cd_3As_2, Nat. Commun. **7**, 10301 (2016).